International Forum on Aeroelasticity and Structural Dynamics
IFASD 2024
17-21 June 2024, The Hague, The Netherlands

COMPARISON BETWEEN COMPUTATIONAL AND EXPERIMENTAL NON-STATIONARY PRESSURE DISTRIBUTION ON A PITCH-OSCILLATING WING

Bruno de A. Regina[1], **Roberto G. A. da Silva**[1], **Eduardo S. Molina**[2]

[1]Instituto Tecnológico de Aeronáutica
Praça Marechal Eduardo Gomes, 50, Vila das Acacias, São José dos Campos, SP, 12228-900, Brazil
brunoar9@gmail.com
gil@ita.br

[2]EMBRAER S.A.
São José dos Campos, SP, 12227-901, Brazil
eduardo.molina@embraer.com.br

Keywords: Unsteady aerodynamics, Aeroelasticity, CFD

Abstract: The objective of this work is to obtain CFD results for the dynamic response of a wing oscillating in pitch in a transonic regime using an open-source tool. The purpose is to verify and improve the correspondence with the experimental data as performed in the wind tunnel test for a wing model developed by Embraer. For this, in some analyzes it is proposed to impose a prescribed movement to the wing in the CFD simulations that models the bending observed in the scaled model throughout the tests as a rigid mesh movement in rolling direction. Prescribed motion parameters are extracted directly from the model's structural deformation measurement data. In addition, simulations of a test case using the Benchmark Supercritical Wing (BSCW) are performed to investigate the impact of relevant variables in this type of analysis, such as time step and mesh refinement level. The time step was identified as the most influential parameter to approximate the simulation results to experimentally obtained data. The CFD results for the Embraer wing were able to capture the main behaviors of the magnitude and phase of the non-stationary pressure coefficient on the wing, mainly for conditions of higher reduced frequencies, with an affordable computational cost.

1 INTRODUCTION

As the world advances in its quest for increased efficiency, the aeronautical industry is increasing its interest in lightweight wings, which inadvertently brings the structure closer to its stiffness limits. One of the undesired consequences of this approach on the projects is the challenge related to aeroelasticity. The interaction between aerodynamic, elastic and inertial forces in an unsteady scenario can provide positive feedback to the amplitude of the wing's movement and possibly lead to structural destruction [1].

Several initiatives have come up to better understand the aeroelastic phenomena. Since 2012 three AIAA Aeroelastic Prediction Workshops (AePW) have been held, so as to assess the state-of-the-art computational aeroelasticity, evaluating the effectiveness of the current modeling techniques and algorithms and further identifying the fields both computationally and experimentally which still require research and development [2–4].

To investigate the unsteady aerodynamics of a typical Embraer commercial aircraft wing, transonic wind tunnel tests were carried out as reported by [5]. The main purpose of the experiments was to measure the non-stationary pressure distribution of a wing model with forced pitch oscillations, providing valuable information regarding aeroelastic phenomena for the selected geometry and the analyzed flight conditions. Different values of Mach number and oscillating frequencies were assessed in the tests.

In this context, this work aims to refine the preliminary Computational Fluid Dynamics (CFD) results obtained by [5] solving Reynolds Averaged Navier-Stokes equations, attempting to better match them with the available wind tunnel data. This is done by applying a dynamic movement on the wing which models the bending oscillations which were observed on the wind tunnel tests and were not considered on the fluid dynamic simulations performed on said paper.

But first, a test case is used to validate the software, the post-processing codes and the methodology, simulating the unsteady dynamics of the Benchmark Supercritical Wing (BSCW) which was originally proposed on the 2^{nd} AePW.

2 THEORETICAL FORMULATION

For an airfoil oscillating in pitch, the incidence is subject to:

$$\alpha = \alpha_0 + \Delta\alpha \cos \omega t \tag{1}$$

where α_0 is the mean angle, $\Delta\alpha$ is the oscillation magnitude and ω is the angular frequency. This airfoil motion is responsible for the emergence of an unsteady pressure which is added to the average local pressure p_s as a sinusoidal component.

$$p = p_s + \Delta p = p_s + p_1 \cos(\omega t + \varphi) \tag{2}$$

where Δp is the unsteady pressure component, p_1 is the magnitude of the pressure perturbation and φ is the phase angle, in relation to the original α oscillation. The reduced frequency k is an important flow similarity parameter which can be used to quantify unsteady flows around oscillating airfoils.

$$k = \frac{2\pi f c_{ref}}{2V} \tag{3}$$

where f is the oscillating frequency in Hertz, c_{ref} is the reference chord of the airfoil (mean aerodynamic chord) and V is the flow velocity.

The pressure coefficients along an oscillating airfoil can be analyzed in the frequency domain, by the use of Frequency Response Functions (FRFs). They are relationships of output and input between the C_p and the angle of attack α at the excitation frequency, with each of those variables having been through a Fast Fourier Transform (FFT) [5].

The FFT applied on the pressure coefficients along the wing surface is calculated by solving:

$$\hat{x}_d(f) = \sum_{n=-N}^{N} x_n e^{-i2\pi f n \Delta t} \tag{4}$$

where Δt is the sampling time, N is the total number of samples used in the signal and x_n is equivalent to the C_p values obtained from the simulation.

3 SU2 SOFTWARE

The software chosen in this work for the Computational Fluid Dynamics simulations is the SU^2 (or Stanford University Unstructured), which is an open-source collection of tools programmed in Python and C++ to solve PDEs and PDE-constrained optimization [6]. Based on the Finite Volume Method (FVM), it can run on general, unstructured meshes, which ensures flexibility when working with complex geometries. The software's foundation is a Reynolds-averaged Navier-Stokes (RANS) solver, able to solve compressible and turbulent flows, but also capable of computing several multi-physics problems. Applying a rigid body movement or a prescribed structural motion to the analyzed body is made possible through its Arbitrary Langrangean-Eulerian approach.

The governing equations are discretized spatially in the FVM with standard edge-based structure on a dual grid with control volumes built using a median-dual, vertexbased scheme [7]. The evaluation of the flow variables gradients may be done with the aid of the Green-Gauss method, averaging the calculated values in all cell nodes to obtain the gradients in each cell face. For the temporal discretization, several implicit and explicit methods are available, and the dual time-stepping approach is used when dealing with time-accurate simulations, with the Flexible Generalized Minimal Residual (FGMRES) scheme being one of the possibilities to solve the temporal equations. The Spalart-Allmaras turbulence model is used in this work.

4 BSCW ANALYSES

For the BSCW validation simulations, the wing is set on a sinusoidal pitch motion going between 2° and 4° of angle of attack in transonic flow. The supersonic region grows and withers according to the incidence angle, affecting the unsteady pressure distribution on the wing surface. Tables 1 to 3 present the parameters used for setting up the simulations.

Table 1: BSCW simulation freestream parameters.

Parameter	Value	Unit
Reynolds, Re_∞	4.56×10^6	$-$
Mach, M_∞	0.70	$-$
Temperature, T_∞	302.98	K
Density, ρ_∞	1.2886	kg/m^3
Viscosity, μ_∞	1.85×10^{-5}	$N.s/m^2$
Heat Capacity Ratio, γ	1.113	$-$
Gas Constant, R	81.49	$J/kg.K$

The pressure coefficient distributions are analyzed in a section at 60% of the BSCW wing span (at $487.7\ mm$ from its root), as proposed in the 2^{nd} AePW, to enable the data comparison between the works here described. Figure 1a represents the airfoil in this reference section. Figure 1b presents the average C_P distribution along the BSCW surfaces, comparing five different analyses: simulations with 64 and 256 steps per period (also called $64p$ and $256p$, respectively),

Table 2: BSCW simulation oscillation parameters.

Parameter	Value	Unit
Mean AoA, α_0	3.0	deg
AoA Variation, $\Delta\alpha$	1	deg
Angular Frequency, ω	62.83	rad/s
Reduced Frequency, k	0.220	–

Table 3: BSCW simulation time step parameters.

Parameter	64p	256p	[8]	Unit
Steps per period	64	256	500	–
Time Step, Δt	0.0015625	0.000390625	0.0002	s

each one with a Coarse and a Medium mesh configuration (the Coarse with $8,392,899$ and the Medium with $27,326,713$ cells on the computational domain), and the results obtained by [8]. The transonic regime in which the simulations occur lead to the appearance of a shock wave on the upper surface of the airfoil, near its leading edge, which causes a sudden surge and then drop of pressure.

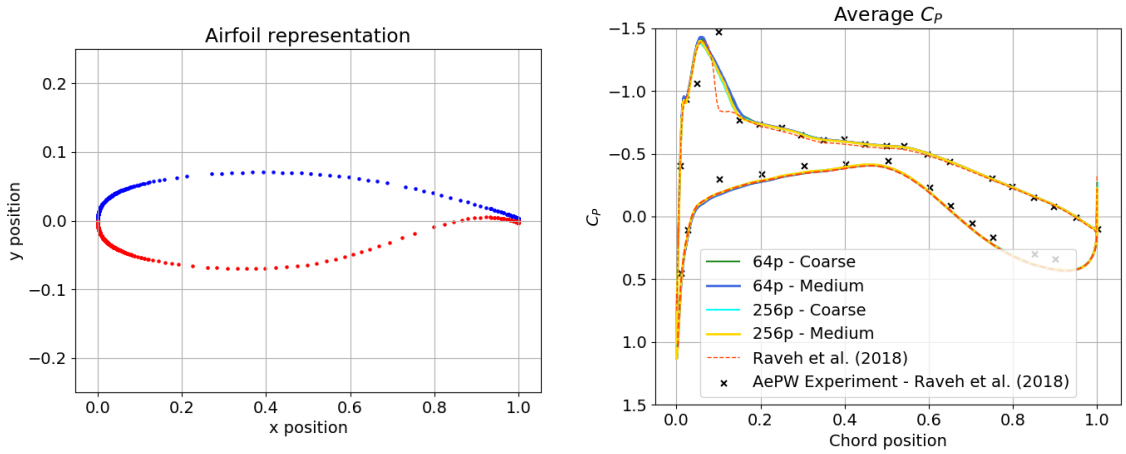

(a) Airfoil representation.

(b) Average pressure coefficient along the surface of the analyzed BSCW section.

Figure 1: Representation of the airfoil on the analysed BSCW section and results for the average pressure coefficient along its surface.

Figures 2a and 2b show the magnitude of the unsteady C_p on the upper and lower surfaces of the BSCW in its reference section, respectively. Changing the mesh configuration from coarse to medium does not seem to bring relevant changes to the amplitude behavior. The smaller time steps were efficient in bringing the results closer to those found in the literature, both in the areas near the shock wave and beyond the 25% chord position, in which there is less pressure variations. The two regions with larger magnitude in pressure fluctuation are the leading edge and the locations close to the oscillating shock wave. Both regions are related to sudden flow deceleration: the first due to the direct influence of the AoA variation and the latter due to the return of the stream to a subsonic regime at the end of the shock wave.

Figures 3a and 3b show the phase of the C_P oscillations on the upper and lower surfaces of the section of interest of the BSCW, respectively, when compared to the wing sinusoidal incidence

variation which originates the unsteady pressures. On the upper surface, the phase angle is soon disturbed by the leading edge and shock wave effects. After the end of the shock wave, this parameter suffers a smooth and consistent variation. The main dynamics in the unsteady C_P phase angle are captured similarly by all of the compared simulations, albeit the $256p$ analyses shows closer relation to the results obtained in [8]. As for the lower surface, the unsteady pressure coefficient phases are well-behaved and show no abrupt variations, except for the region close to its trailing edge. The five simulations present the same nature in their results, but it can be seen that the finer temporal refinement does play a role in maintaining this calculated parameter closer to the literature data. No relevant change in results is observed regarding mesh configuration.

The similarities in the SU^2 results and the one found in the bibliography for the BSCW serve as validation for the methodology, software and post-processing codes, which are also used in later portions of this work.

5 EMBRAER WING MODEL

The focus of this section is on the Embraer Wing Model (EMB-WM). The model used in the simulations is based on the model specified by Embraer, manufactured by NLR (Netherlands

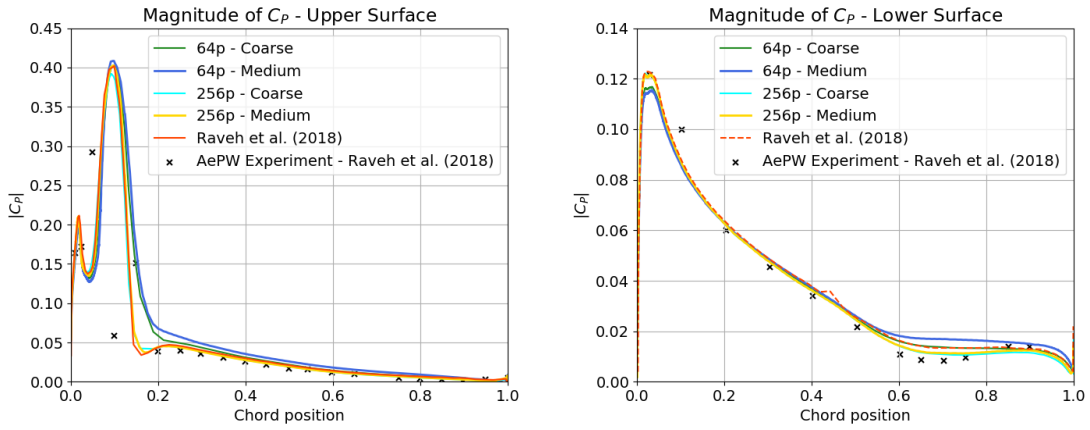

(a) (b)

Figure 2: Magnitude of C_P in the (a) upper and (b) lower surface of the analyzed BSCW section.

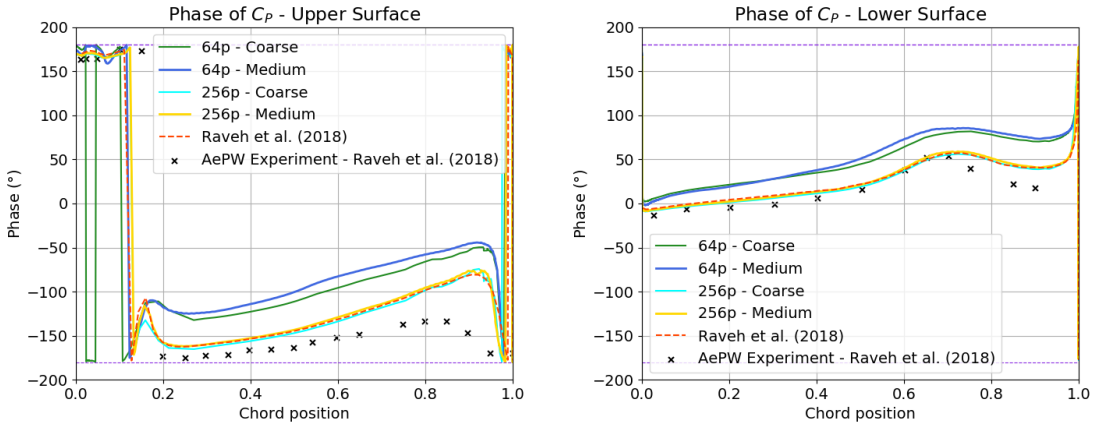

(a) (b)

Figure 3: Phase of C_P in the (a) upper and (b) lower surface of the analyzed BSCW section.

Aerospace Centre) and tested by DNW (German-Dutch Wind Tunnels) on wind tunnel tests, as described in more detail in [5].

The EMB-WM is a scaled model representing half-span of a commercial aircraft wing and a fairing, and it was prepared to perform steady and unsteady aerodynamics tests. It is attached to a disk which can be rotated to set the desired angle-of-attack to the model, and an oval disk set on the lateral side of the fairing has a small gap which allows the oval disk (along with the wing) to rotate in pitch motion and to move in the vertical axis, according to the aerodynamic loads acting on the EMB-WM. This gap is what enables the unsteady aerodynamics testing to be performed.

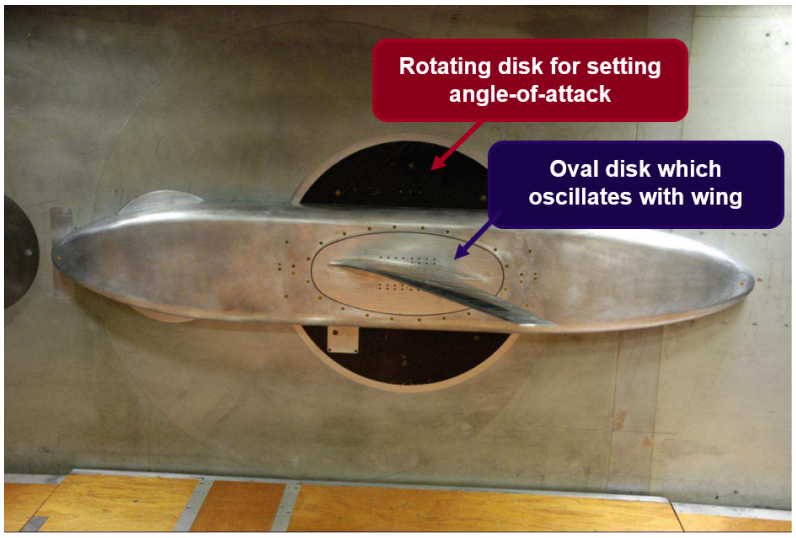

Figure 4: EMB-WM test setup mounted in the wind tunnel. Source: adapted from [5].

The EMB-WM was equipped with accelerometers, optical markers and pressure transducers, these last positioned in specific wing sections and responsible for capturing the C_P information during steady and unsteady tests. Using a Stereo Pattern Recognition (SPR) system, the optical markers are used to provide information on vertical displacement and twist of the studied wing sections.

5.1 Steady analyses

The first set of simulations performed on the EMB-WM are steady analyses, where the lift coefficient of the wing is verified for different angles of attack in $M_\infty = 0.8$ condition and compared to bibliography ([5]) and experimental data to ensure that the model is faithfully represented in the SU^2 software. Table 4 presents the freestream parameters considered in the simulations on the EMB-WM analyses.

Table 4: EMB-WM simulation freestream parameters.

Parameter	Value	Unit
Reynolds, Re_∞	3.0×10^6	–
Mach, M_∞	0.80	–
Temperature, T_∞	293.2	K
Heat Capacity Ratio, γ	1.4	–
Gas Constant, R	287.059	$J/kg.K$

The computational domain has a semi-spherical shape with the model in the middle of the flat

wall that serves as a symmetry plane. The unstructured mesh is formed of $17,533,444$ cells and $6,583,128$ points, being coarser near its outer limits and getting progressively finer when approaching the model. It was created following the gridding guidelines for self-generated meshes from the 7^{th} AIAA Drag Prediction Workshop [9]. The grid was based on the same computational domain used by [5], which also does not represent the wind tunnel walls and has no internal arbitrary mesh interface which could enable some cell regions to move while others keep completely static on the simulation. The mesh used represents the model already deformed by the dynamic pressure acting on the wing (model on flight shape). This helps to bring the simulation conditions closer to what was actually observed in practice during the wind tunnel tests.

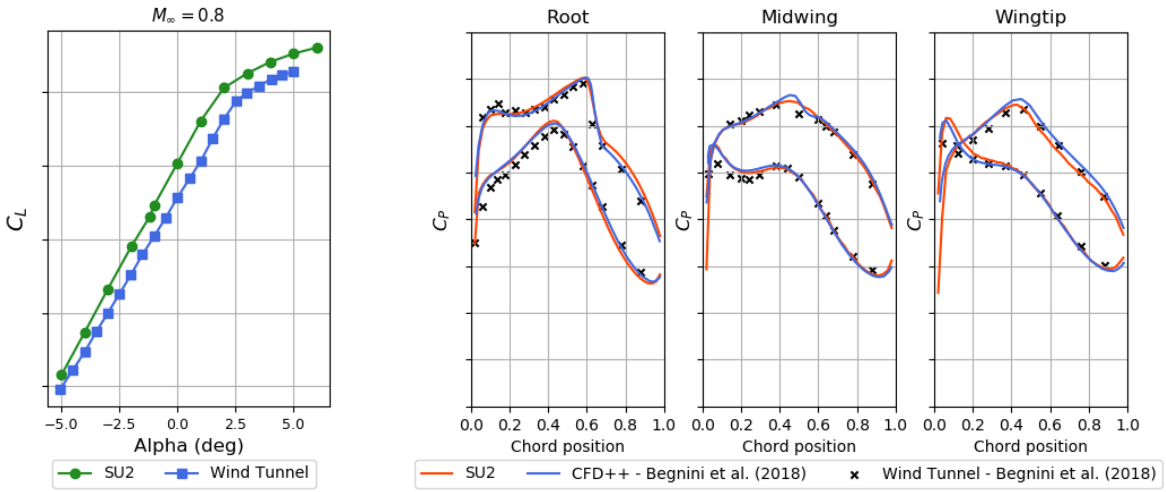

(a) (b)

Figure 5: Graphs comparing the CFD and Experimental (a) CL x alpha curves for $M_\infty = 0.8$ and (b) pressure distributions on different wing sections at $M_\infty = 0.8$ for same C_L condition.

On Figure 5a it can be seen that there is a certain difference between the values obtained through CFD and the experimental data, and it is as if the curves were with a shift in the angle-of-attack. A possible cause for this deviation could be the effect of the wind tunnel walls in the experimental results, which is not considered in the CFD simulations. The C_{L_α} derivative seems to diverge between the simulated and measured curves in some of the angle-of-attack regions. But the overall good agreement between the curves' main trends are seen as positive evidence that the simulation parameters are coherent.

The unsteady analyses in the following sections are based on the EMB-WM oscillating in pitch with an initial angle-of-attack condition of -0.5 degrees. The flow characteristics and the respective pressure conditions it generates on the wind tunnel model when set in this AoA are an important input for the CFD simulations (more important than the actual AoA parameter, in fact), and quite relevant to be well captured on the steady analyses, as they are used as initial condition for the unsteady cases. Therefore, due to the shift in angle-of-attack observed in the lift coefficient curve on Figure 5a, a -1.2 degrees angle-of-attack was input as the initial EMB-WM angle-of-attack condition on the SU^2 simulations, instead of the -0.5 degrees of experimental wind tunnel tests.

With this AoA delta to match C_L there is a good matching between the pressure distribution results from the SU^2 simulations, the data obtained through commercial CFD software on [5]

and the experimental wind tunnel results, as can be seen in Figure 5b. The characteristic sudden pressure drop of a shock can be seen near the wing root. Between different sections, the pressure coefficients go through changes related to wing geometry (torsion and taper, for example) and three-dimensional wing tip effects, reducing the total lift generated further away from the wing root.

Based on the results from this section, it can be concluded that the mesh used on the SU^2 simulations is representative of the one which was used on the work of 5 and of the flow conditions on the EMB-WM wind tunnel tests. The mesh was validated for the steady case and, based on the AePW simulation results from section 4, it is argued that the use of a more refined mesh would not be justified. For a mesh which already captures the main behavior of the flow as precisely as this one, the benefits of a further refinement would be marginal when compared to the increased computational costs.

5.2 Forced Pitch Oscillations Analysis

For the EMB-WM unsteady simulations in this work, flow conditions of $M_\infty = 0.8$ is studied, using the converged flow results from the steady computations as initial conditions for the simulations. Furthermore, reduced frequencies of 0.05 and 0.25 are studied and compared in the analyses, to verify how much the pitch oscillation frequency affects the unsteady pressures on the wing surface. As in [5], the whole mesh is set to oscillate in a rigid body motion, including the fairing. This is a computationally cost-effective method to model the oscillations, as alternatives for this have extra computations related to mesh deformation or for passing information through interfaces between static and dynamic portions of the grid. Table 5 presents the oscillation parameters considered in the simulations on the unsteady EMB-WM analyses.

Table 5: EMB-WM simulation oscillation parameters.

Parameter	Value	Unit
Mean AoA, α_0	-1.2	deg
AoA Variation, $\Delta\alpha$	0.35	deg

The simulations using forced pitch oscillations consider a fixed number of 128 time steps per cycle, the same value used by [5]. Three cycles of oscillation were simulated and used for post-processing.

5.2.1 Forced Pitch Oscillations Analysis with Bending

This section describes the modeling of bending oscillations which are introduced as a representation of prescribed structural motion on the EMB-WM simulations, in addition to the already applied pitch motion. A comparison is made in subsection 5.3 between the 'Pitch-only' simulation results, the 'Pitch and Bending' and the results obtained in [5]. The bending motion is modeled through an imposed rolling oscillation to the body, making the wing tip move vertically with a certain amplitude and frequency. The idea is that the upward and downward movement at the analyzed frequencies is responsible for inducing relative flow velocities in the model, especially at the regions closer to the wing tip, which have greater amplitude of motion. These relative flow velocities affect the effective angle-of-attack alongside the wing sections, possibly having an impact on the pressure coefficient distribution on them.

Figure 6a shows a representation of the wing bending as seen from a front view. The wing structure can be represented as a cantilever beam attached to the fairing, and the vertical bending

displacements along the sections vary smoothly until the final value of dz at the wingtip. To model such a motion on the simulations, it would be necessary to add mesh recalculations at each time step, increasing significantly the computational effort for them to be completed. This structural bending motion can be modeled as an imposed rolling oscillation to the whole EMB-WM, making the wing tip move upwards and downwards with the same dz amplitude it would have on the original bending condition, emulating therefore the change in the effective angle-of-attack along the wing sections (Figure 6b).

As can be seen when comparing Figure 6a and 6b, the rolling approximation for the vertical displacements on the wing is more representative of the actual bending movement when analysing the wing sections closer to the tip. In addition to the more expressive vertical movement at the root of the wing, the whole fairing is also set to move alongside the rest of the model, which disturbs the portions of the flow closer to it. That is not, however, expected to impact the results significantly. That is because of the small lever arms the regions closer to the wing root present when comparing to the motion origin, which lead to small vertical velocities (and consequently, a small variation to the section's effective angle-of-attack).

Data obtained during the wind tunnel tests (Figure 7) are used to set the rolling motion parameters of amplitude and frequency on the CFD analyses. Using information gathered by the SPR markers closer to the wing tip it was possible to analyse their vertical displacement during a complete cycle of the driver signal (the forced pitch oscillations). An averaged value for the dz of the leading and trailing edge SPR markers was considered to compensate for the effects of pitching twist in the section. Having the information of maximum vertical displacement and span position in which the SPR markers are placed, simple trigonometric relations are used to

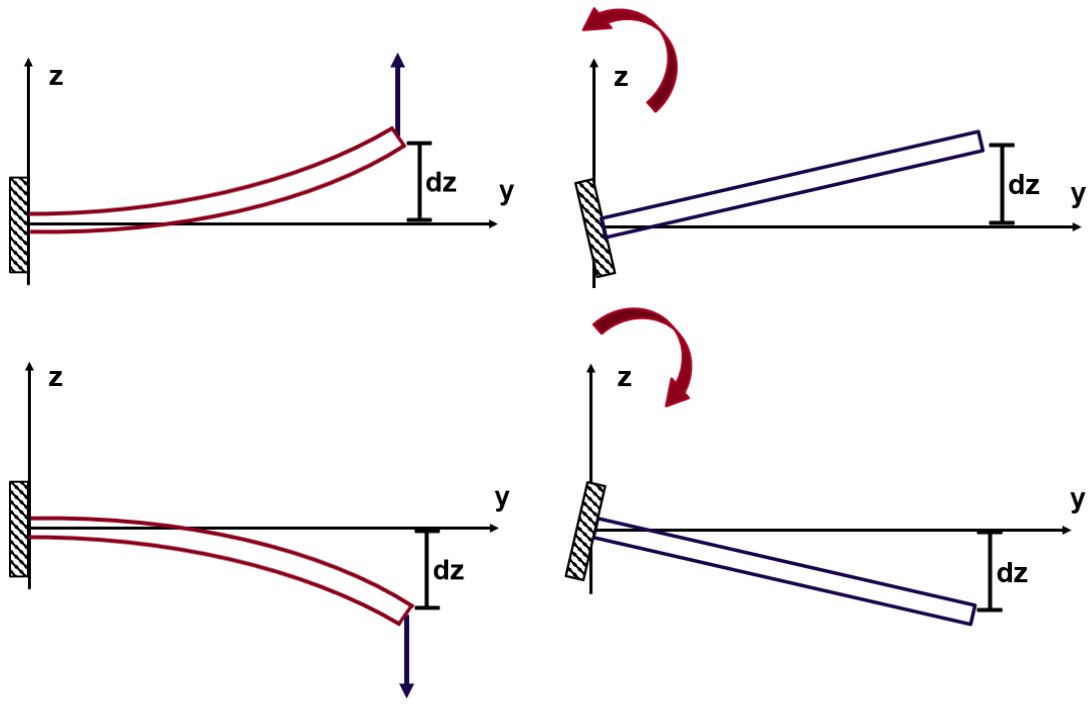

(a) (b)

Figure 6: Schematics of the (a) bending oscillations on a wing and (b) how it was modeled as roll mesh oscillations on the simulations.

get the amplitude (in degrees) of the rolling oscillation. As for the frequency of the rolling vibrations, it can be seen in the SPR results presented in Figure 7 that the vertical displacement mainly follows the dynamics of the driver signal. The forced pitch oscillations cause cyclic variations to the wing's C_L, which in turn generate cyclic bending motion on the model's structure in the same frequency.

Instead of 128 time steps per cycle, 256 time steps per cycle were used on the forced pitch oscillations with bending simulations. This helps ensure that small disturbances on the flow are well captured on the simulation, and that the computations do not diverge. Other than that and the rolling motion itself, the main simulation conditions run for this section are the same as the ones described in the previous section.

5.3 EMB-WM Unsteady Simulation Results

The results for the unsteady EMB-WM conditions are presented in this section, varying the reduced frequency between the lower and upper values (0.05 and 0.25, respectively). The images in the next few pages show a comparison between the SU^2 analyses with both 'Pitch-only' and 'Pitch and bending' conditions with the computational and experimental data presented by [5].

The unsteady C_P distributions are shown on reference wing sections, discretized between the upper and lower surface of the model for each analysed condition. The graphs in a same figure have the same scales in the vertical axis for each row of results, to better enable comparisons between results from the different wing sections. Magnitude and phase results of the Frequency Response Functions in each section are presented one above the other, which helps to visualize the overall unsteady pressure characteristics along the chord.

The phase of the FRF is presented in an unwrapped manner in this section, to allow comparison with the data obtained by [5]. The unwrapped phase basically means that when the angle reaches $\pm 180°$, it won't be represented with a sudden drop or surge in its values, as seen in Figure 3a, for example. Instead, it will follow a more natural representation for the variation of this parameter, based on trigonometric equivalence between angles 360 degrees apart.

Figure 8 shows the unsteady pressure distribution along the reference sections for the $M_\infty = 0.8$ and $k = 0.05$ condition. As is quite evident on the magnitude and phase graphs, especially near the wing root on the upper surface, there are shock regions on this analysed case. The

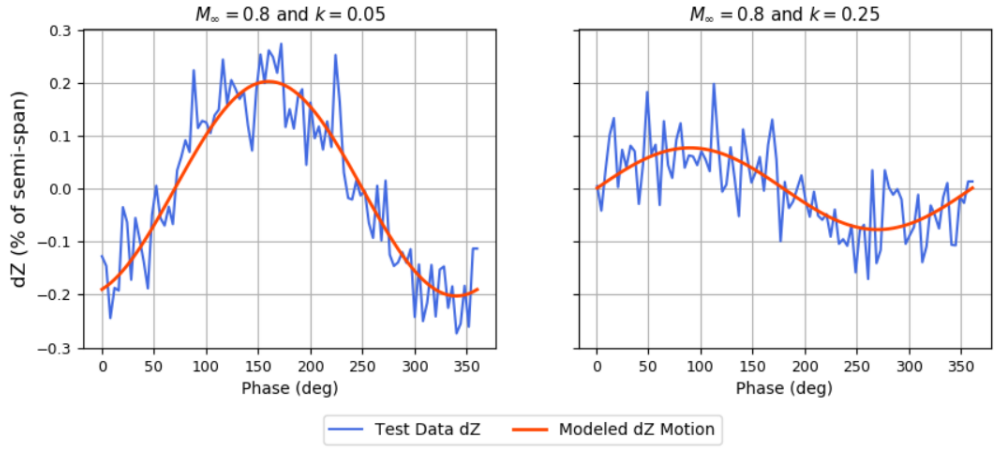

Figure 7: Wingtip SPR vertical displacement and modeled movement for different k conditions.

sudden pressure variations in a small longitudinal chord distance is characteristic of the shock oscillations along the model's surface. The position of the shock waves are well captured on the simulations when compared to wind tunnel results.

Analysing the magnitude of the FRF on the upper and lower surfaces, it can be verified that the SU^2 results considering 'Pitch and bending' had smaller values when compared to data from other simulations. The main suspicion is that the smaller frequency analysis are also related to higher amplitudes in the bending movement (Figure 7), and that this increase in the rolling angles ends up affecting the pressure distributions for the analyses. The decrease in the magnitude for the 'Pitch and bending' simulation makes it fare better on the upper and lower surfaces near the root, getting closer to the experimental data in several chord regions. This is not applicable to the other wing sections, however, as it is seen that this analysis ends up underestimating the C_P/α magnitudes.

SU^2 simulations weren't able to capture shock strength on the wing tip quite as well as the computational analysis found on the literature [5]. Despite that, all of the computational analyses are able to capture the main behavior of the magnitudes relatively well, specially on the lower surface of the wing, which is also considerably more uneventful than the upper surface, as no shock is seen past the region close to the root.

Regarding the phase results, it seems that the 'Pitch and bending' analysis stands out on the upper surface, approaching the experimental points behavior better than the other computational analyses, especially for the sections further away from the root. The SU^2 analysis with 'Pitch-only' performs well close to the root, but does not maintain this behavior when approaching the wing tip. Worth mentioning, however, is the fact that the upper and lower surface curves detach from the experimental data mainly on the trailing edge, in regions where the magnitude of the pressure is really small and therefore can lead the phase to inadvertently deviate from the expected in the presence of small pressure disturbances. The CFD++ results seen on the

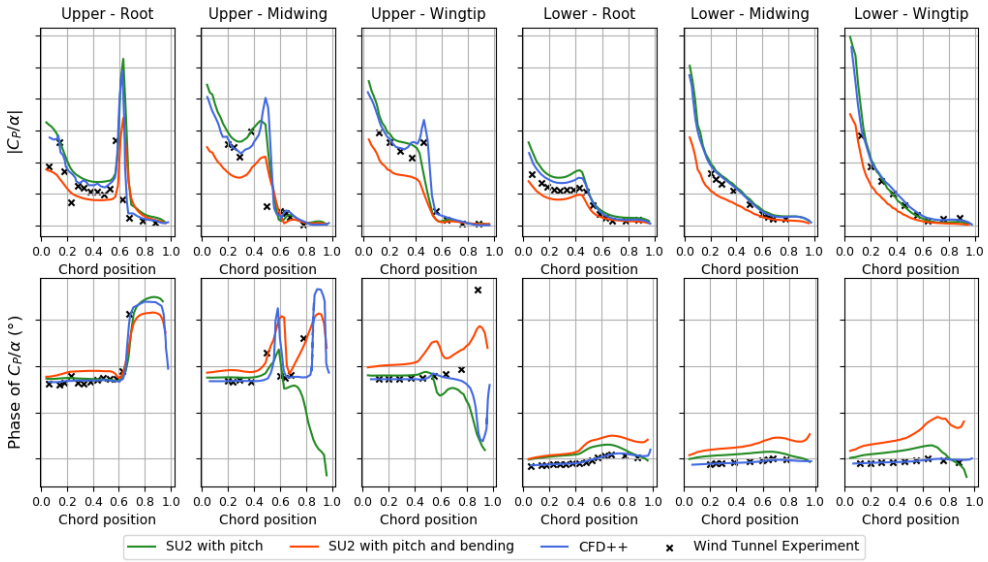

Figure 8: EMB-WM unsteady pressure coefficients on the upper surface for the $M_\infty = 0.8$ and $k = 0.05$ condition.

literature, on the other hand, is able to capture the wind tunnel data behavior quite well on the lower surface .

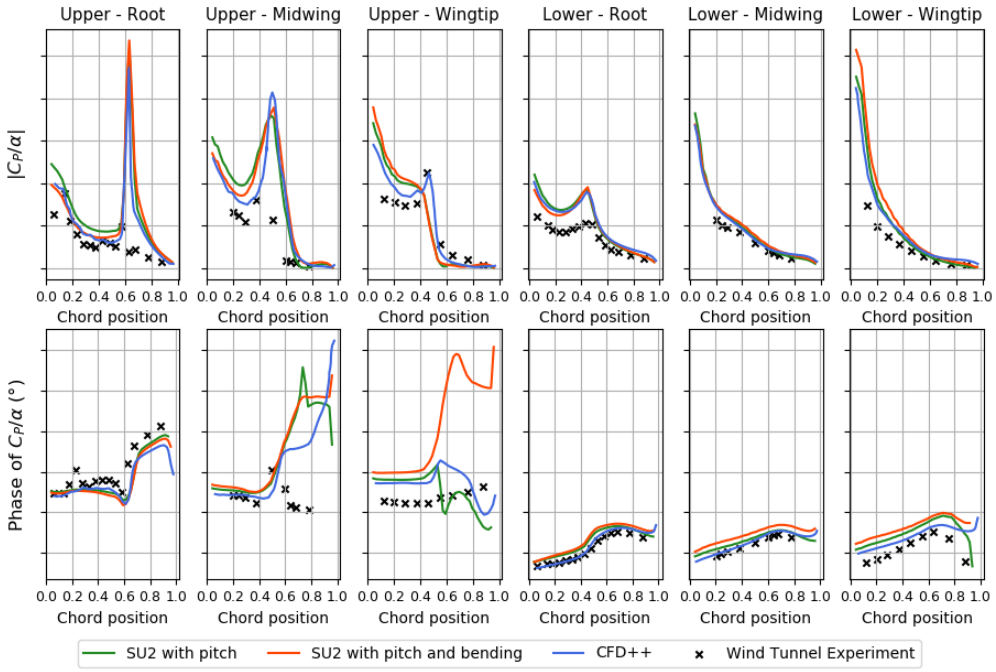

Figure 9: EMB-WM unsteady pressure coefficients on the upper surface for the $M_\infty = 0.8$ and $k = 0.25$ condition.

Figure 9 presents the unsteady pressure distribution along the reference wing sections for the $M_\infty = 0.8$ and $k = 0.25$ condition. Once again the shock presence is evident on the results, with sudden pressure variations marking the regions within the limits of the shock wave oscillations. Supersonic zones mainly appear along the upper surface, but lower root section also develops a small one.

There is a possibility that the wind tunnel experiment used too few pressure transducers on each section to be able to capture relevant information. Although there is a great agreement between the position of the shock waves in both computational and experimental results, the pressure amplitude due to shock isn't always captured on the wind tunnel data. It is not clear whether there could be a stronger shock happening in upper root and midwing sections (as suggested by the simulation results), for example, and the small number of data acquisition points prevents this to be shown on the experimental outcomes.

The upper and lower magnitude results obtained computationally were able to follow the main dynamics from the experimental data, but all of the simulations overestimated the pressure along the wing model. The simulation outcomes are quite similar with one another, overall, and this is specially the case in the lower surface.

As for the phase of C_P/α, it can be seen that, for the upper midwing and wingtip sections, none of the verified computational analyses were able to capture the expected behavior of the results. Although rather stable values for the phase were measured on these sections closer to the wing tip, the calculated results on the simulations had difficulties approaching them.

This was not a problem on the upper root section, however. On the lower surface the phase results main behavior was well captured, but the experimental and computational curves begin gradually distancing themselves, with the phase shift of each of the simulations with respect to wind tunnel data increasing when approaching the wing tip. If not for the phase shift, the SU^2 'Pitch-only' simulation would be the one to better approach experimental results.

6 CONCLUSIONS AND FUTURE WORK

The analyses presented in this work show the relevance of studying the unsteady aerodynamics of airfoils and wings in transonic flow regime. Small variations on the angle of attack can lead to considerable changes on the pressure distributions along the wing surfaces. When subject to aeroelastic phenomena such as the transonic SDOF flutter, these incidence variations occur dynamically, affecting the shock wave position and strength and the overall flow behavior. Imposing pitch oscillations on a wing can be a relevant method of studying the subject both experimentally and through computational means. Having robust numerical tools which are able to predict correctly these effects end up being a great asset on the process of aircraft design.

The SU^2 software shows to be a powerful tool for the CFD simulations, solving compressible flows alongside multi-physic problems in a quick and efficient way. The open-source tool was able to provide relevant information for the analyses, which could be correlated with experimental data. Such is the case for the shock positions and the overall magnitudes behavior on the EMB-WM unsteady analyses, for example, as well as the pressure distribution along the wing model on the EMB-WM steady analyses.

Along the results presented it was possible to observe that there were some discrepancies between experimental and simulation results, and there are many possible reasons for them. Both on the BSCW and on the EMB-WM analyses the computational model did not include a representation of wind tunnel walls, for example. The tunneling effect has an impact on flow velocities, modifying the effective angle-of-attack along the wing model. For steady analyses, corrections can be applied to mitigate the absence of the tunnel walls on the simulations. But things may not be as straightforward on the unsteady case, as the flow dynamics change continuously, and therefore also the pressure distributions along the model.

Furthermore, in both of BSCW and EMB-WM cases the whole mesh was set to oscillate as a rigid body motion. This possibly creates more divergence between the results in the EMB-WM analysis, because the fairing is also represented on the computational model used in the analyses, and setting it to oscillate creates a situation which is not completely in agreement with what was done on the experiments. As can be seen on Figure 4, the fairing was kept completely static on the wind tunnel tests, with only a region close to the wing being allowed to move due to the imposed oscillations and vertical displacements due to the aerodynamic loads. It would be expected that this oscillating fairing effect would create more of an impact along sections closer to the wing root, however, and what was seen on the results is that even near the wing tip there are still divergences on the results between simulations and experiments.

It was argued by [8] that the discrepancy between the simulation and test data in the 10% chord area in the BSCW analysis is due to pressure measurements points being very few and scattered in the experiment. This same issue may have happened on the EMB-WM analyses. For $M_\infty = 0.8$, where great pressure variations occur along small portions of the wing chord due to shock oscillations, some of the discrepancies between tunnel data and simulations can possibly be explained by this effect. Upper sections results on Figure 8 and Figure 9 are examples, specially

on the higher reduced frequency case, where experimental data did not show the magnitude surges on the C_P near shock regions properly.

For lower reduced frequencies, the SU^2 with 'Pitch and bending' FRF magnitudes were reduced, an effect that is possibly related to how the movement was modeled. When looking at the SPR data, the lower reduced frequency conditions were related to higher bending displacements, but also higher pitching twist along the sections near the wing tip, which can have great impact on the pressure distribution variations and wasn't considered on the simulations. As one can see when comparing Figure 6a and Figure 6b, it was expected that the addition of the rolling motion modeling the wing bending could create extra disturbances near the wing root (due to the rolling effects of the fairing and wing sections near the root itself), but compensate with a better performance near the wing tip (where the vertical displacement would come closer to what was seen on the SPR data). But the lack of torsion dynamics on the simulations possibly interferes negatively on this region, preventing the CFD outcomes to approach the experimental results.

The relatively low-cost simulations using rigid motion on the mesh in the form of rolling oscillations to model the bending dynamics of the wing model were considered a valid test to verify if computational and experimental data could get closer to one another. The results weren't conclusive in this regard, though. The wing sections closer to the tip presented greater deviations to the measured pressure distributions than the sections near the wing root. It was believed that the wing flexibility was responsible for those differences, as the sensors measuring structural movement detected higher dynamic response when higher frequencies were being studied, but that didn't seem to be the case (at least not in the way that the wing flexibility was implemented in this work). Of course, one thing to be considered is the fact that the modeling of the bending movement as rigid mesh motion has limitations as no wing torsion dynamics is considered, and that can also affect local angle-of-attack significantly.

Other conclusion that can be obtained through the BSCW analyses in this work is that when the mesh is already sufficiently adequate for the considered problem, refinements don't seem to be effective means to approximate unsteady C_P simulation results to experimental data, as they add more computational cost than improve the result itself. Additionally, the time step showed to be an important parameter to get better fidelity of the non-stationary results. The use of large time-steps can compromise the simulation's capacity of capturing finer unsteady flow patterns, sometimes affecting the quality of the analysis outcomes.

7 ACKNOWLEDGEMENTS

The authors would like to gratefully acknowledge Embraer for providing experimental data and computational resources, essential for the development of this research.

The authors wish to express their gratitude to the São Paulo Research Foundation, FAPESP, which has supported the present research under the Research Grants No. 21/11258-5. The authors also gratefully acknowledge the support for the present research provided by Conselho Nacional de Desenvolvimento, CNPq, under the Research Grant No. 309985/2013-7

8 REFERENCES

[1] Tijdeman, H. (1977). Investigations of the transonic flow around oscillating airfoils. *NLR-TR 77090 U*.

[2] Heeg, J., Ballmann, J., Bhatia, K., et al. (2011). Plans for an aeroelastic prediction workshop.

[3] Heeg, J., Chwalowski, P., Schuster, D., et al. (2015). Plans and example results for the 2nd aiaa aeroelastic prediction workshop. In *56th AIAA/ASCE/AHS/ASC Structures, Structural Dynamics, and Materials Conference*. p. 0437.

[4] Chwalowski, P., Massey, S. J., Jacobson, K., et al. (2022). Progress on transonic flutter and shock buffet computations in support of the third aeroelastic prediction workshop. In *AIAA Scitech 2022 Forum*. p. 1347.

[5] Begnini, G. R., Bones, C. A., and Spode, C. (2018). Transonic wind tunnel test of wing oscillating in pitch. In *2018 Applied Aerodynamics Conference*. p. 3004.

[6] Palacios, F., Economon, T. D., Aranake, A., et al. (2014). Stanford university unstructured (su2): Analysis and design technology for turbulent flows. In *52nd Aerospace Sciences Meeting*. p. 0243.

[7] Economon, T. D., Palacios, F., Copeland, S. R., et al. (2016). Su2: An open-source suite for multiphysics simulation and design. *AIAA Journal*, 54(3), 828–846.

[8] Raveh, D. E., Mor Yossef, Y., and Levy, Y. (2018). Analyses for the second aeroelastic prediction workshop using the eznss code. *AIAA Journal*, 56(1), 387–402.

[9] Vassberg, J. (2022). Drag prediction workshop - vii: Baseline rans grid family plan. 7th AIAA CFD Drag Prediction Workshop.

COPYRIGHT STATEMENT